

Topological phases protected by projective PT symmetry in alkaline-earth-like atoms

Xiaofan Zhou,^{1,2} Suotang Jia,^{1,2} and Jian-Song Pan^{3,4,*}

¹*State Key Laboratory of Quantum Optics and Quantum Optics Devices,
Institute of Laser Spectroscopy, Shanxi University, Taiyuan 030006, China*

²*Collaborative Innovation Center of Extreme Optics,
Shanxi University, Taiyuan, Shanxi 030006, China*

³*College of Physics, Sichuan University, Chengdu 610065, China*

⁴*Key Laboratory of High Energy Density Physics and Technology of
Ministry of Education, Sichuan University, Chengdu 610065, China*

An important aspect in categorizing topological phases is whether the system is spinless or spinful, given that these classes exhibit distinct symmetry algebras, leading to disparate topological classifications. By utilizing the projective presentation strategy, the topological phases of spinless (or spinful) systems can be emulated using spinful (or spinless) systems augmented with gauge fields. In this study, we propose to implement the topological phases safeguarded by the unique projective space-time (PT) symmetry inherent to spinful models, using synthetic spinless alkaline-earth-like atoms. Employing the separation of orbital and nuclear-spin degrees of freedom, the model is configured as a rectangular tube penetrated by a uniform magnetic flux through each plaquette, which simulates a spinless ladder endowed with projective PT symmetry satisfying the algebraic properties of a spinful model. For interacting topological phases with inter-orbital spin-exchange interactions, which also adhere to PT symmetry, the four-fold degeneracy of edge modes is split into two pairs of edge modes with two-fold degeneracy. We map the complete phase diagram in the end and discover that these interacting topological phases ultimately evolve into distinct charge-density-wave phases via spontaneous symmetry breaking.

I. INTRODUCTION

Topological phases in free systems can generally be classified based on their internal and spatial group symmetries [1–13]. The fundamental distinction in topological classification hinges on whether the systems being examined are spinful or spinless. These two spin categories exhibit distinct topological phases, originating from their differing symmetry algebra [14]. A prime example is the spacetime inversion symmetry, denoted as PT symmetry [15, 16]. In spinful systems, $(PT)^2 = -1$, resulting in a Kramers double degeneracy throughout the Brillouin zone (BZ). In contrast, spinless systems have $(PT)^2 = 1$, ensuring a real band structure. Thus, the spin class inherently determines the topological phases that a physical system can manifest.

Recent theoretical advancements have shown that the traditional limitations in topological classification can be surpassed in the presence of gauge symmetry [17]. Specifically, the space inversion symmetry P can be projectively represented as $\mathcal{P} = GP$ [18, 19], where G is a gauge transformation. By carefully selecting G , the projective PT symmetry can be tailored to satisfy $(\mathcal{PT})^2 = 1$ in spinful systems or $(\mathcal{PT})^2 = -1$ in spinless systems. This enables the realization of topological phases that were previously exclusive to either spinless or spinful systems in the opposite category. Notably, spinful topological phases have now been observed in inherently spinless acoustic crystals [20]. These findings open up new avenues for exploring novel topological phases beyond the

conventional topological classification [21].

So far, the aforementioned studies have focused on single-particle physics, overlooking the crucial role of many-body interactions. Interactions are essential in topological phases, as they can, for example, introduce zeros in the single-particle Green's function and disrupt the bulk-boundary correspondence between topological invariants and edge states. Conversely, while additional symmetries can suppress perturbations that share those symmetries, it is believed that topological phases protected by more symmetries are more robust against perturbations due to their increased structural complexity. Therefore, investigating interacting topological phases protected by projective PT symmetry holds significant theoretical importance. Ultracold atoms in optical lattices naturally interact with each other, and their interaction strength can be precisely tuned using Feshbach resonance [22–24]. This makes ultracold atoms in optical lattices an outstanding platform for studying interacting topological phases in condensed matter physics.

In this study, we propose to realize spinful topological phases using a synthetic spinless optical lattice clock, with synthetic dimensions implemented by nuclear and orbital degrees of freedom [25–32]. Particularly, with the help of interactions within the clock-state manifolds controlled via the orbital Feshbach resonance [33–35], we can study the impact of interaction on the topological phases protected by projective PT symmetry. These interactions lead to the splitting of the four-fold degenerate ground-state entanglement spectra into two-fold degeneracy. When further increasing the interaction strengths, the interacting topological phases are driven into different order phases with spontaneous symmetry breaking.

* panjsong@scu.edu.cn

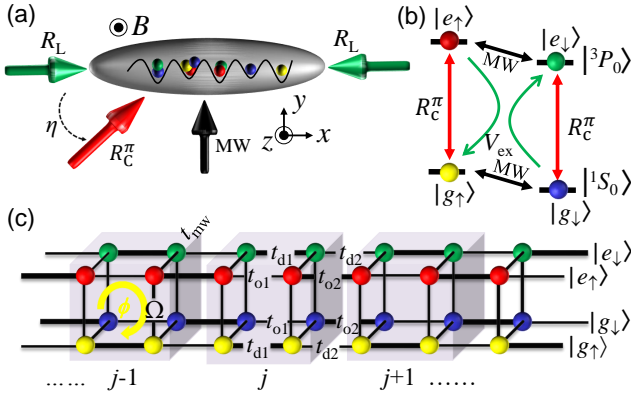


FIG. 1. Illustration of the proposed model. (a) Ultracold alkaline-earth-like atoms are loaded onto one-dimensional (1D) spin-dependent optical superlattices created by a series of interfering laser beams denoted by R_L . A narrow π -polarized clock laser, R_C^π , induces a single-photon transition between the clock-state manifolds within the same hyperfine spin states. By adjusting the angle η between the clock laser and the laser generating the optical lattice, the photon recoil momentum can be tuned as $k_C = 2\pi/\lambda_C \cos \eta$ and thus the phases carried by the coupling terms are tunable. Microwaves (MW) are employed to couple the two hyperfine spin states. (b) Energy level diagram and relevant coupling. The two hyperfine spin states are coupled by microwaves. States within the $|^1S_0\rangle$ and $|^3P_0\rangle$ manifolds are coherently coupled by the spin-conserving clock laser (R_C^π , indicated by the red curves). Additionally, interactions within the clock-state manifolds can couple different spin states across different orbitals (depicted by the green curves). (c) Configuration for the tight-binding model of the 1D optical clock. It consists of a square tube with four legs (namely, $|g \uparrow\rangle$, $|e \uparrow\rangle$ and $|g \downarrow\rangle$, and $|e \downarrow\rangle$), where each on-page plaquette is penetrated by the same synthetic magnetic flux $\phi = \pi\lambda_L/\lambda_C \cos \eta$. Gray cubes represent the unit cells of the configuration, while colored spheres represent the sites.

We numerically map the phase diagram and propose that the interaction-induced topological phase transitions can be explored by measuring the local occupation of clock states at the edges. Our research pioneers the exploration of topological phases protected by projective PT symmetry in the realm of ultracold atoms.

The rest of this paper is structured as follows. In section II, we elaborate the quantum simulation framework under consideration. Section III provides the definitions of the quantities employed to characterize the topological phases and phase transitions. The details of the interacting topological phases and interaction-induced phase transitions are presented in section IV. Finally, a brief summary is given in section V.

II. QUANTUM SIMULATION SCHEME

We propose to investigate the switching between interacting spinless and spinful topological phases using the

following model:

$$\begin{aligned}
 \hat{H} = & - \sum_{j,\alpha\sigma}^{g\uparrow,e\downarrow} (t_{d1} \hat{c}_{2j-1\alpha\sigma}^\dagger \hat{c}_{2j\alpha\sigma} + t_{d2} \hat{c}_{2j\alpha\sigma}^\dagger \hat{c}_{2j+1\alpha\sigma} + \text{H.c.}) \\
 & - \sum_{j,\alpha\sigma}^{g\downarrow,e\uparrow} (t_{o1} \hat{c}_{2j-1\alpha\sigma}^\dagger \hat{c}_{2j\alpha\sigma} + t_{o2} \hat{c}_{2j\alpha\sigma}^\dagger \hat{c}_{2j+1\alpha\sigma} + \text{H.c.}) \\
 & + \Omega \sum_{j,\sigma} (e^{i\phi_j} \hat{c}_{jg\sigma}^\dagger \hat{c}_{je\sigma} + \text{H.c.}) + t_{mw} \sum_{j,\alpha} (\hat{c}_{j\alpha\uparrow}^\dagger \hat{c}_{j\alpha\downarrow} + \text{H.c.}) \\
 & + U \sum_j (\hat{n}_{jg\uparrow} \hat{n}_{je\downarrow} + \hat{n}_{jg\downarrow} \hat{n}_{je\uparrow}) + U_0 \sum_{j\sigma} \hat{n}_{jg\sigma} \hat{n}_{je\sigma} \\
 & + V_{ex} \sum_j (\hat{c}_{jg\uparrow}^\dagger \hat{c}_{je\downarrow}^\dagger \hat{c}_{je\uparrow} \hat{c}_{jg\downarrow} + \text{H.c.}), \tag{1}
 \end{aligned}$$

where $\hat{c}_{j\alpha\sigma}$ ($\hat{c}_{j\alpha\sigma}^\dagger$) denotes the annihilation (creation) operator for an atom on the j th site of the $\alpha = e, g$ orbital with spin $\sigma = \uparrow, \downarrow$, and $\hat{n}_{j\alpha\sigma} = \hat{c}_{j\alpha\sigma}^\dagger \hat{c}_{j\alpha\sigma}$. This Hamiltonian is formulated in the context of alkaline-earth-like atoms on an optical clock lattice. Note that the term ‘‘spinless’’ does not imply the absence of atomic spin degrees of freedom; rather, it indicates that the Hamiltonian adheres to a PT symmetry algebra of spinless systems, i.e., $(PT)^2 = 1$, where the two hyperfine spin states are treated as two spatial degrees of freedom, constituting a synthetic spatial dimension. Consequently, the Hamiltonian describes a one-dimensional spatial tube [Fig. 1(c)]. Due to staggered longitudinal hopping, each unit cell comprises 8 sites. The Ω hopping terms include a site-dependent phase, equivalent to a constant flux piercing the on-page plaques. The interaction terms are associated with orbital Feshbach resonances.

An optical clock lattice can be created by loading atoms into a series of one-dimensional (1D) spin-dependent optical superlattice potentials. They can be achieved by interfering laser beams (R_L) at specific ‘tune-out’ wavelengths [see Fig. 1(a)], ensuring that atoms in the state α, σ are exclusively confined by the lattice potential $V_{\alpha,\sigma}^L$ and not influenced by other potentials [36, 37]. The spin- and orbital-dependence is accomplished by using lasers with different frequencies and circular polarizations to couple the hyperfine states in distinct orbitals to higher energy levels. The superlattice is formed by the superposition of a background lattice and an additional lattice with twice the lattice constant.

The spin-conserved Ω term, is realized using an ultranarrow π -polarized clock laser (R_C^π) with a wavelength λ_C [see Fig. 1(a)]. This laser drives a single-photon transition between the clock states $|g\rangle$ and $|e\rangle$, which share the same nuclear spins σ ($|\uparrow\rangle$ or $|\downarrow\rangle$) [see Fig. 1(b)]. The angle η between the wave vector of the clock laser and the 1D optical lattice [see Fig. 1(a)] results in a momentum transfer of $k_C = 2\pi/\lambda_C \cos \eta$. By adjusting η , we can tune the site-dependent phase of the Ω terms. To couple the two spin states $|\uparrow\rangle$ and $|\downarrow\rangle$ [see Fig. 1(b)], we propose using microwaves (MW) [37]. When the 1D optical lattice is sufficiently deep and the Rabi frequency of the clock

laser is not excessively large [38–40], the single-band approximation becomes valid, allowing us to formulate the tight-binding model as described above.

Under this setup, the longitudinal spin-conserving hopping coefficients are given by $t_{\alpha\sigma,jj+1} = \left| \int dx w^{(j)} \left[-\frac{\nabla^2}{2m} + V_{\alpha,\sigma}^L(x) \right] w^{(j+1)} \right|$, with $w^{(j)}$ being the lowest-band Wannier function at the j th site of the background lattice potential. Here we have assumed that the background lattice potentials and thus the Wannier functions are the same for different orbitals and hyperfine spins. The double-well potentials are designed to obtain $t_{g\uparrow,2l2l+1} = t_{e\downarrow,2l2l+1} = t_{o1}$, $t_{e\uparrow,2l2l+1} = t_{g\downarrow,2l2l+1} = t_{d1}$, $t_{g\uparrow,(2l+1)(2l+1)+1} = t_{e\downarrow,(2l+1)(2l+1)+1} = t_{o2}$, and $t_{e\uparrow,(2l+1)(2l+1)+1} = t_{g\downarrow,(2l+1)(2l+1)+1} = t_{d2}$. The spin-conserving coupling coefficient $\Omega e^{i\phi j} = \Omega_R \int dx w^{(j)} e^{ik_C x} w^{(j)}$, in which Ω_R is the Rabi frequency of the clock laser. Here $\phi = \frac{1}{2}k_C \lambda_L = \pi \lambda_L / \lambda_C \cos \eta$ is the synthetic flux penetrating each on-page plaquette, where λ_L is the wavelength of the lasers generating the background lattice. For the interaction part, $U = \frac{1}{2}(g_+ + g_-) \int dx w^{(j)} w^{(j)} w^{(j)} w^{(j)}$, and $U_0 = g_- \int dx w^{(j)} w^{(j)} w^{(j)} w^{(j)}$ measures the inter-orbital density-density interaction strengths with the same and different nuclear spins, respectively. $V_{\text{ex}} = \frac{1}{2}(g_- - g_+) \int dx w^{(j)} w^{(j)} w^{(j)} w^{(j)}$ is the inter-orbital spin-exchange interaction strength.

The Hamiltonian (1) offers the advantage of allowing independent tuning of all its parameters. Specifically, $t_{\alpha\sigma,jj+1}$ can be adjusted by modifying the depth of the optical lattice potential, while Ω and ϕ can be controlled via the Rabi frequency and the angle of the clock laser, respectively. Additionally, the parameters $\{V_{\text{ex}}, U, U_0\}$ can be fine-tuned using orbital Feshbach resonance [33–35] or confinement-induced resonance [41, 42]. Subsequently, we set $U_0 = V_{\text{ex}} + U$, as determined by the scattering parameters of ^{173}Yb atoms [41, 42].

The single-particle part of Hamiltonian (1) is formulated based on the one-dimensional single-particle models presented in Refs. [17, 20], thereby inheriting the same symmetrical framework. We fix the flux $\phi = \pi$ to ensure that each plaquette perpendicular to the x direction experiences a π flux. The coupling strengths, given by $\Omega e^{i\phi j}$, alternate between positive and negative values for neighboring links, specifying a \mathbb{Z}_2 gauge field where $\mathbb{Z}_2 = \{\pm 1\}$. A gauge transformation G applied to this \mathbb{Z}_2 gauge field, through $\hat{c}_{j\alpha\downarrow} \rightarrow -\hat{c}_{j\alpha\downarrow}$, maintains the flux configuration intact.

The space inversion symmetry operation (P) is executed by interchanging the spins \uparrow and \downarrow , the orbitals g and e , and the sites j and $-j$. It's worth emphasizing that, in this framework, the two spin degrees of freedom are regarded as spatial degrees of freedom. As a result, the space-time inversion symmetry adheres to the relation $(PT)^2 = 1$, which is characteristic of spinless PT-symmetric models. Although the flux configuration is unchanged for the spatial reversion transformation, the

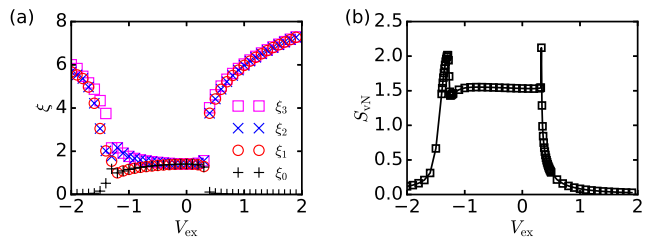


FIG. 2. Variations of entanglement spectrum and von Neumann entropy. (a) The lowest four levels in the entanglement spectrum ξ_i ($i = 1, 2, 3, 4$), and (b) the von Neumann entropy S_{vN} as functions of V_{ex} with $U = 0.0$, $L = 56$ and $\rho = 0.5$ under open boundary conditions.

gauge connection and thus the Hamiltonian are changed. In fact, due to the presence of the \mathbb{Z}_2 gauge symmetry, the Hamiltonian submits to the projective space inversion symmetry $\mathcal{P} = GP$. However, the projective space-time inversion symmetry fulfills $(PT)^2 = -1$, thereby determining the spinful algebra and topological classifications, although we start with a synthetic spinless model.

The 1D topologically gapped phase belongs to the DIII class of spinful models. We set the parameters as follows: $t_{d1} = t_{o2} = 0.2 - \Delta_t$, $t_{d2} = t_{o1} = 0.2 + \Delta_t$, $\Omega = 0.1$ and $t_{\text{mw}} = 0.1$. The Hamiltonian (1) features four Kramers double-degenerate bands and two Majorana Kramers pairs of topological boundary modes, which are localized at one end of the chain and guaranteed by the projective PT symmetry with $(PT)^2 = -1$. The winding number of the chain is constrained to even integers, denoted as $2Z$ [17]. The band gap closes at $\Delta_t = 0$, marking a topological phase transition. To study the topological insulator properties of interacting fermions, we focus on the case where $\Delta_t = 0.1$. At half filling, where $\rho = N/4L = 0.5$, the lower four bands and two zero modes are occupied, resulting in the ground state exhibiting topological insulating behavior with edge states. To quantitatively explore the topological properties of the model, we employ the state-of-the-art DMRG numerical method [43, 44]. We consider a lattice length up to $L = 56$ at half filling ($\rho = 0.5$). For our calculations, we retain 400 truncated states per DMRG block and perform 30 sweeps, achieving a maximum truncation error of approximately $\sim 10^{-10}$.

III. QUANTITIES FOR CHARACTERIZING INTERACTING TOPOLOGICAL PHASES

The topological states and phase transitions in strongly correlated systems generally can be characterized by the entanglement spectrum, entanglement entropy, and excited energy gap. The entanglement spectrum is defined as follows [45]:

$$\xi_i = -\ln(\rho_i), \quad (2)$$

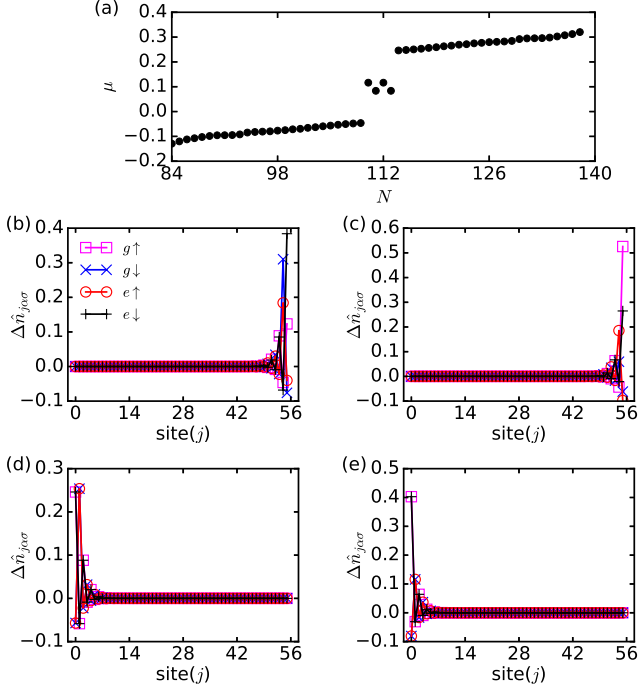


FIG. 3. Chemical potential and edge modes. (a) Chemical potential $\mu(N)$ for a chain with $L = 56$ lattice sites under open boundary conditions. (b)-(e) The edge-mode density distributions $\Delta \hat{n}_{j\alpha\sigma}$ of the four mid-gap modes for the TI state. Here, $V_{\text{ex}} = 0.2$ and $U = 0.0$.

where ρ_l represents the eigenvalues of the reduced density matrix $\hat{\rho}_l = \text{Tr}_{L-l} |\psi\rangle\langle\psi|$, with $|\psi\rangle$ being the ground state. Here, l denotes the length of the left block in a specific bipartition. A system is considered topologically nontrivial if its entanglement spectrum exhibits degeneracy, as this degeneracy is indicative of the presence of edge excitations [45–51].

The quantum criticality of interaction-driven topological phase transitions can be characterized by the von Neumann entropy [51–56]:

$$S_{\text{vN}} = -\text{Tr}_l [\hat{\rho}_l \log \hat{\rho}_l], \quad (3)$$

where $l = L/2$. A divergence in the von Neumann entropy at the critical point signifies a continuous transition. The central charge of the conformal field theory describing the critical behavior can be extracted from the asymptotic behavior of the entanglement entropy, which reflects the universality class of the phase transition. For a critical system with open boundary conditions, the von Neumann entropy of a subchain of length l scales as:

$$S_{\text{vN}}(l) = \frac{c}{6} \ln \left[\sin \left(\frac{\pi l}{L} \right) \right] + \text{const}, \quad (4)$$

where the slope at large distances gives the central charge c of the conformal field theory [57–60].

For the TI phase under open boundary conditions, a notable characteristic is the emergence of localized edge

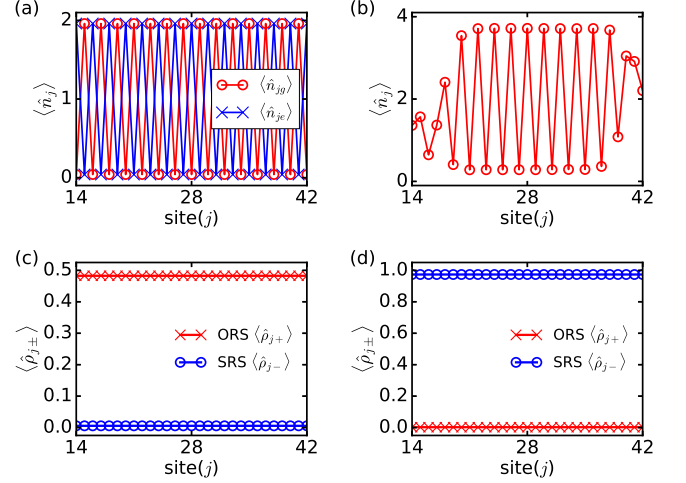


FIG. 4. Order parameters induced by interaction. (a) The density distribution $\langle \hat{n}_{j\alpha} \rangle$ in ODW phase with $V_{\text{ex}} = 0.0$ and $U = 1.8$. (b) $\langle \hat{n}_j \rangle$ in CDW phase with $V_{\text{ex}} = -0.2$ and $U = -0.6$. (c) The local order parameter $\langle \hat{\rho}_{j\pm} \rangle$ in ORS phase with $V_{\text{ex}} = -1.9$ and $U = 1.0$. (d) $\langle \hat{\rho}_{j\pm} \rangle$ in the SRS phase with $V_{\text{ex}} = 1.5$ and $U = 0.15$. Here, $L = 56$ and $\rho = 0.5$.

modes. These topological edge modes manifest within the bulk energy gap and can be identified from the chemical potential spectrum corresponding to different occupations. The chemical potential spectrum is defined as:

$$\mu(N) = E_0(N+1) - E_0(N), \quad (5)$$

representing the energy needed to add an atom to a system comprising N atoms. Here, $E_0(N)$ denotes the ground-state energy for a system with N atoms under open boundary conditions. The density distribution of the edge modes can be computed using:

$$\Delta \hat{n}_{j\alpha\sigma} = \langle \hat{n}_{j\alpha\sigma}(N+1) \rangle - \langle \hat{n}_{j\alpha\sigma}(N) \rangle, \quad (6)$$

where $\langle \hat{n}_{j\alpha\sigma}(N) \rangle$ represents the density distribution for a system with N atoms.

The exchange interactions can lead to various order states with spontaneous symmetry breaking, including the rung-singlet states, the charge-density wave (CDW) state, and the orbital-density wave (ODW) state, by evaluating their respective local orders [61–63]. The singlet states within the orbital (or spin) degrees of freedom are defined as $|\pm\rangle = (|g\uparrow; e\downarrow\rangle \pm |g\downarrow; e\uparrow\rangle)/\sqrt{2}$ and can be distinguished through the corresponding local order parameter:

$$\langle \hat{\rho}_{j\pm} \rangle = |\pm\rangle\langle\pm|. \quad (7)$$

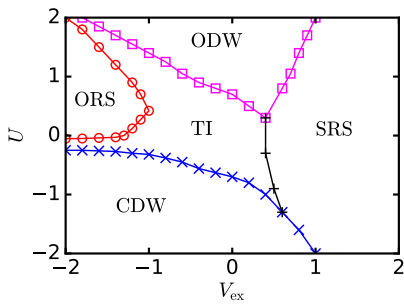


FIG. 5. The phase diagram of Hamiltonian (1) on $V_{\text{ex}} - U$ plane with half filling $\rho = 0.5$ in the thermodynamic limit, which contains TI (topological insulator), SRS (spin rung-singlet), ORS (orbital rung-singlet), ODW (orbital density wave) and CDW (charge density wave) phases.

IV. INTERACTION DRIVEN TOPOLOGICAL PHASE TRANSITIONS

In the absence of interactions, the system behaves as a topological insulator (TI). Here, we investigate the effect of increasing the spin-exchange interaction V_{ex} while keeping U fixed at zero. When $V_{\text{ex}} = 0$, the eigenstates in the entanglement spectrum exhibit a fourfold degeneracy. However, this degeneracy is partially lifted in the presence of a weak V_{ex} . As the interaction strength V_{ex} is further increased, the degeneracy of ξ_i is completely lifted beyond a critical repulsive (attractive) interaction strength of $V_{\text{ex}}^c \sim 0.35(-1.25)$, as illustrated in Fig. 2(a). Additionally, the von Neumann entropy S_{vN} displays sharp peaks near these two critical points, as shown in Fig. 2(b).

For the single-particle topological insulator (TI) state, mid-gap modes corresponding to the four topological edge modes (two for each orbital) appear in the chemical-potential spectrum. These mid-gap modes signify the excitation energies needed as the occupation number of the edge modes incrementally rises from zero to four. Nonetheless, when there is a finite interaction strength, such as $V_{\text{ex}} = 0.2$, these mid-gap modes shift towards the bulk, as depicted in Fig. 3(a). As the interaction strength increases further, the mid-gap modes ultimately merge into the bulk spectrum. The edge modes exhibit localized density distributions at the edges, as illustrated in Figs. 3(b) through 3(e).

As the interaction strengths are further increased, multiple trivial order phases arise. Figure 4 indicates that, for the repulsive V_{ex} case with $U = 0$, the trivial symmetric state is the spin rung-singlet (SRS) state [63]. This state can be described by the direct-product state $\prod_i |-\rangle_i$. When U becomes non-zero, the system can transition into the orbital rung-singlet (ORS) state ($\prod_i |+\rangle_i$), the charge-density wave (CDW) state, or the orbital-density wave (ODW) state, depending on the topological phase boundaries. Both the CDW and ODW states are trivial ordered states characterized by spontaneously bro-

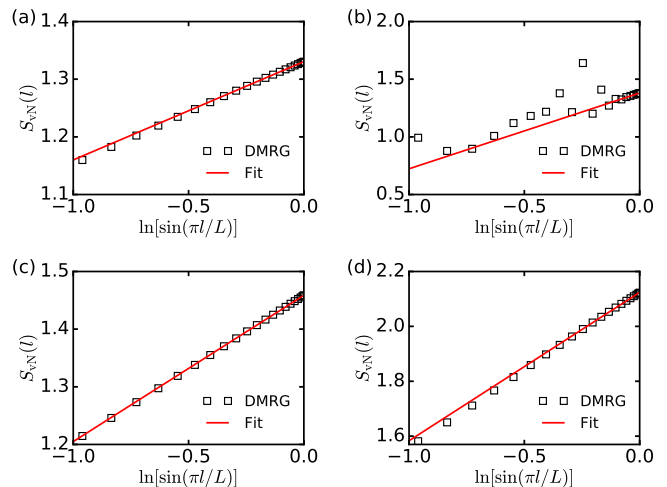


FIG. 6. The scaling of von Neumann entropy $S_{\text{vN}}(l)$ as function of $\ln[\sin(\pi l/L)]$ at critical points. The red solid lines are the linear fit with: $S_{\text{vN}} = c/6 \ln[\sin(\pi l/L)] + \text{const}$. The central charge c is six times the slope of the linear fit. (a) The T \rightarrow ODW phase boundary with $V_{\text{ex}} = 0.0$ and $U = 0.51$, $c \sim 1.0$. (b) The T \rightarrow CDW phase boundary with $V_{\text{ex}} = 0.0$ and $U = -0.514$, $c \sim 3.94$. (c) The T \rightarrow ORS phase boundary with $V_{\text{ex}} = -1.0$ and $U = 0.6$, $c \sim 1.5$. (d) The T \rightarrow SRS phase boundary with $V_{\text{ex}} = 0.335$ and $U = 0.0$, $c \sim 3.2$. Here, $L = 56$ and $\rho = 0.5$.

ken chiral symmetry, which can be verified by computing the relevant local quantities as shown in Fig. 4.

Utilizing the entanglement spectrum ξ_i , von Neumann entropy S_{vN} , order parameter calculations, and finite-size scaling, we have constructed the phase diagram in the thermodynamic limit, as depicted in Fig. 5. The numerical results suggest that the critical points for phase transitions remain consistent across various finite lattice sizes L .

The system behaves as Luttinger liquids at the phase boundaries. As illustrated in Fig. 6, by analyzing the divergence of the von Neumann entropy at these boundaries, we have determined that the central charges for the T-ODW, T-CDW, T-ORS, and T-SRS phase transitions are approximately 1.0, 3.94, 1.5, and 3.2, respectively. These critical points delineate several lines that serve as the phase boundaries between the quantum phases. These lines represent Luttinger liquids with varying central charges, as depicted in Fig. 5.

V. CONCLUSIONS

In this paper, we first present a detailed quantum simulation scheme for exploring spinful topological phases in optical lattices of synthetic spinless alkaline-earth-like atoms. Next, we numerically characterize the topological phase, and discuss the impact of interactions. Our findings reveal that interactions lift the four-fold degen-

eracy of edge modes into a two-fold degeneracy. As interaction strengths further increase, various order phases with spontaneous symmetry breaking arise. Lastly, we present a comprehensive phase diagram that encompasses both the interacting spinful topological phase and the interaction-induced order phases.

ACKNOWLEDGMENTS

X.Z. and S.J. are supported by National Key Research and Development Program of China under Grant No.

2022YFA1404201, the National Natural Science Foundation of China (NSFC) under Grant Nos. 12174233, 12004230 and 12034012, the Research Project Supported by Shanxi Scholarship Council of China and Shanxi “1331KSC”. J.S.P. is supported by the Science Specialty Program of Sichuan University under Grant No. 2020SCUNL210 and the Fundamental Research Funds for the Central Universities under Grant No. YJ202212.

-
- [1] D. J. Thouless, M. Kohmoto, M. P. Nightingale, and M. den Nijs, Quantized Hall conductance in a two-dimensional periodic potential, *Phys. Rev. Lett.* **49**, 405 (1982).
- [2] C. L. Kane, and E. J. Mele, Quantum Spin Hall Effect in Graphene, *Phys. Rev. Lett.* **95**, 226801 (2005).
- [3] B. A. Bernevig, and S.-C. Zhang, Quantum Spin Hall Effect, *Phys. Rev. Lett.* **96**, 106802 (2006).
- [4] B. A. Bernevig, T. L. Hughes, and S.-C. Zhang, Quantum spin Hall effect and topological phase transition in HgTe quantum wells, *Science* **314**, 1757–1761 (2006).
- [5] J. E. Moore, and L. Balents, Topological invariants of time-reversal-invariant band structures, *Phys. Rev. B* **75**, 121306 (2007).
- [6] M. König, S. Wiedmann, C. Brune, A. Roth, H. Buhmann, L. W. Molenkamp, X.-L. Qi, S.-C. Zhang, Quantum spin Hall insulator state in HgTe quantum wells, *Science* **318**, 766–770 (2007).
- [7] D. Hsieh, D. Qian, L. Wray, Y. Xia, Y. S. Hor, R. J. Cava and M. Z. Hasan, A topological Dirac insulator in a quantum spin Hall phase, *Nature* **452**, 970–974 (2008).
- [8] M. Z. Hasan, and C. L. Kane, Colloquium: topological insulators, *Rev. of Mod. Phys.* **82**, 3045–3067 (2010).
- [9] X. L. Qi, and S. C. Zhang, Topological insulators and superconductors, *Rev. of Mod. Phys.*, **83**, 1057 (2011).
- [10] M. Z. Hasan, and J. E. Moore, Three-dimensional topological insulators, *Ann. Rev. of Cond. Matt. Phys.* **2**, 55–78 (2011).
- [11] P. Hořava, Stability of Fermi surfaces and K theory, *Phys. Rev. Lett.* **95**, 016405 (2005).
- [12] Y. X. Zhao and Z. D. Wang, Topological classification and stability of Fermi surfaces, *Phys. Rev. Lett.* **110**, 240404 (2013).
- [13] J. Kruthoff, J. de Boer, J. van Wezel, C. L. Kane, and R.-J. Slager, Topological classification of crystalline insulators through band structure combinatorics, *Phys. Rev. X* **7**, 041069 (2017).
- [14] C. Chiu, J. Teo, A. Schnyder, and S. Ryu, Classification of topological quantum matter with symmetries, *Rev. Mod. Phys.* **88**, 035005 (2016).
- [15] A. P. Schnyder, S. Ryu, A. Furusaki, and A. W. W. Ludwig, Classification of topological insulators and superconductors in three spatial dimensions, *Phys. Rev. B* **78**, 195125 (2008).
- [16] Y. X. Zhao, A. P. Schnyder, and Z. D. Wang, Unified theory of PT and CP invariant topological metals and nodal superconductors, *Phys. Rev. Lett.* **116**, 156402 (2016).
- [17] Y. X. Zhao, C. Chen, X. L. Sheng, and S. A. Yang, Switching spinless and spinful topological phases with projective PT symmetry, *Phys. Rev. Lett.* **126**, 196402 (2021).
- [18] S. Bieri, C. Lhuillier, and L. Messio, Projective symmetry group classification of chiral spin liquids, *Phys. Rev. B* **93**, 094437 (2016).
- [19] Y. X. Zhao, Y. X. Huang, and S. A. Yang, Z_2 -projective translational symmetry protected topological phases, *Phys. Rev. B* **102**, 161117 (2020).
- [20] Y. Meng, S. Lin, B. Shi, B. Wei, L. Yang, B. Yan, Z. Zhu, X. Xi, Y. Wang, Y. Ge, S. Yuan, J. Chen, G.-G. Liu, H. Sun, H. Chen, Y. Yang, and Z. Gao, Spinful topological phases in acoustic crystals with projective PT symmetry, *Phys. Rev. Lett.* **130**, 026101 (2023).
- [21] J. Herzog-Arbeitman, Z.-D. Song, N. Regnault, and B. A. Bernevig, Hofstadter topology: noncrystalline topological materials at high flux, *Phys. Rev. Lett.* **125**, 236804 (2020).
- [22] I. Bloch, J. Dalibard, and W. Zwerger, Many-body physics with ultracold gases, *Rev. Mod. Phys.* **80**, 885 (2008).
- [23] M. Lewenstein, A. Sanpera, and V. Ahufinger, Ultracold atoms in optical lattices: simulating quantum many-body systems (Oxford Univ. Press, 2012).
- [24] P. Windpassinger and K. Sengstock, Engineering novel optical lattices. *Rep. Prog. Phys.* **76**, 086401 (2013).
- [25] M. Takamoto, F. L. Hong, R. Higashi, and H. Katori, An optical lattice clock, *Nature (London)* **435**, 321 (2005).
- [26] X. Zhang, M. Bishof, S. L. Bromley, C. V. Kraus, M. S. Safronova, P. Zoller, A. M. Rey, and J. Ye, Spectroscopic observation of SU(N)-symmetric interactions in Sr orbital magnetism, *Science* **345**, 1467 (2014).
- [27] F. Scazza, C. Hofrichter, M. Höfer, P. C. De Groot, I. Bloch, and S. Fölling, Observation of two-orbital spin-exchange interactions with ultracold SU(N)-symmetric fermions, *Nat. Phys.* **10**, 779 (2014); *ibid* **11**, 514 (2015).
- [28] G. Cappellini, M. Mancini, G. Pagano, P. Lombardi, L. Livi, M. Siciliani de Cumis, P. Cancio, M. Pizzocaro, D. Calonico, F. Levi, C. Sias, J. Catani, M. Inguscio, and L. Fallani, Direct observation of coherent interorbital spin-exchange dynamics, *Phys. Rev. Lett.* **113**, 120402 (2014); *ibid* **114**, 239903 (2015).
- [29] M. L. Wall, A. P. Koller, S. Li, X. Zhang, N. R. Cooper, J. Ye, and A. M. Rey, Synthetic spin-orbit coupling in

- an optical lattice clock, *Phys. Rev. Lett.* **116**, 035301 (2016).
- [30] S. Kolkowitz, S. L. Bromley, T. Bothwell, M. L. Wall, G. E. Marti, A. P. Koller, X. Zhang, A. M. Rey, and J. Ye, Spin-orbit-coupled fermions in an optical lattice clock, *Nature (London)* **542**, 66 (2017).
- [31] L. F. Livi, G. Cappellini, M. Diem, L. Franchi, C. Clivati, M. Frittelli, F. Levi, D. Calonico, J. Catani, M. Inguscio, and L. Fallani, Synthetic dimensions and spin-orbit coupling with an optical clock transition, *Phys. Rev. Lett.* **117**, 220401 (2016).
- [32] B. Song, C. He, S. Zhang, E. Hajiyev, W. Huang, X.-J. Liu, and G.-B. Jo, Spin-orbit-coupled two-electron Fermi gases of ytterbium atoms, *Phys. Rev. A* **94**, 061604 (2016).
- [33] R. Zhang, Y. Cheng, H. Zhai, and P. Zhang, Orbital Feshbach resonance in alkali-earth atoms, *Phys. Rev. Lett.* **115**, 135301 (2015).
- [34] G. Pagano, M. Mancini, G. Cappellini, L. Livi, C. Sias, J. Catani, M. Inguscio, and L. Fallani, Strongly interacting gas of two-electron Fermions at an orbital Feshbach resonance, *Phys. Rev. Lett.* **115**, 265301 (2015).
- [35] M. Höfer, L. Riegger, F. Scazza, C. Hofrichter, D. R. Fernandes, M. M. Parish, J. Levinsen, I. Bloch, and S. Fölling, Observation of an orbital interaction-induced Feshbach resonance in ^{173}Yb , *Phys. Rev. Lett.* **115**, 265302 (2015).
- [36] B. Arora, M. S. Safronova, and C. W. Clark, Tune-out wavelengths of alkali-metal atoms and their applications, *Phys. Rev. A* **84**, 043401 (2011).
- [37] Z. Meng, L. Wang, W. Han, F. Liu, K. Wen, C. Gao, P. Wang, C. Chin, and J. Zhang, Atomic Bose-Einstein condensate in twisted-bilayer optical lattices, *Nature* **615**, 231 (2023).
- [38] J.-S. Pan, X.-J. Liu, W. Zhang, W. Yi, and G.-C. Guo, Topological superradiant states in a degenerate Fermi gas, *Phys. Rev. Lett.* **115**, 045303 (2015).
- [39] L. Zhou and X. Cui, Spin-orbit coupled ultracold gases in optical lattices: high-band physics and insufficiency of tight-binding models, *Phys. Rev. B* **92**, 140502(R) (2015).
- [40] J.-S. Pan, W. Zhang, W. Yi, and G.-C. Guo, Bose-Einstein condensate in an optical lattice with Raman-assisted two-dimensional spin-orbit coupling, *Phys. Rev. A* **94**, 043619 (2016).
- [41] M. Olshanii, Atomic scattering in the presence of an external confinement and a gas of impenetrable bosons, *Phys. Rev. Lett.* **81**, 938 (1998).
- [42] R. Zhang, D. Zhang, Y. Cheng, W. Chen, P. Zhang, and H. Zhai, Kondo effect in alkaline-earth-metal atomic gases with confinement-induced resonances, *Phys. Rev. A* **93**, 043601 (2016).
- [43] S. R. White, Density matrix formulation for quantum renormalization groups, *Phys. Rev. Lett.* **69**, 2863 (1992).
- [44] U. Schollwöck, The density-matrix renormalization group, *Rev. Mod. Phys.* **77**, 259 (2005).
- [45] H. Li and F. D. M. Haldane, Entanglement spectrum as a generalization of entanglement entropy: Identification of topological order in non-Abelian fractional quantum Hall effect states, *Phys. Rev. Lett.* **101**, 010504 (2008).
- [46] T. Yoshida, R. Peters, S. I. Fujimoto, and N. Kawakami, Characterization of a Topological Mott insulator in one dimension, *Phys. Rev. Lett.* **112**, 196404 (2014).
- [47] J.-Z. Zhao, S.-J. Hu, and P. Zhang, Symmetry-protected topological phase in a one-dimensional correlated bosonic model with a synthetic spin-orbit coupling, *Phys. Rev. Lett.* **115**, 195302 (2015).
- [48] A. M. Turner, F. Pollmann, and E. Berg, Topological phases of one-dimensional fermions: An entanglement point of view, *Phys. Rev. B* **83**, 075102 (2011).
- [49] F. Pollmann, A. M. Turner, E. Berg, and M. Oshikawa, Entanglement spectrum of a topological phase in one dimension, *Phys. Rev. B* **81**, 064439 (2010).
- [50] L. Fidkowski, Entanglement spectrum of topological insulators and superconductors, *Phys. Rev. Lett.* **104**, 130502 (2010).
- [51] S. T. Flammia, A. Hamma, T. L. Hughes, and X.-G. Wen, Topological entanglement Rényi entropy and reduced density matrix structure, *Phys. Rev. Lett.* **103**, 261601 (2009).
- [52] M. B. Hastings, I. González, A. B. Kallin, and R. G. Melko, Measuring Rényi entanglement entropy in quantum monte carlo simulations, *Phys. Rev. Lett.* **104**, 157201 (2010).
- [53] A. J. Daley, H. Pichler, J. Schachenmayer, and P. Zoller, Measuring entanglement growth in quench dynamics of bosons in an optical lattice, *Phys. Rev. Lett.* **109**, 020505 (2012).
- [54] D. A. Abanin and E. Demler, Measuring entanglement entropy of a generic many-body system with a quantum switch, *Phys. Rev. Lett.* **109**, 020504 (2012).
- [55] H.-C. Jiang, Z.-H. Wang, and L. Balents, Identifying topological order by entanglement entropy, *Nat. Phys.* **8**, 902 (2012).
- [56] R. Islam, R. Ma, P. M. Preiss, M. E. Tai, A. Lukin, M. Rispoli, and M. Greiner, Measuring entanglement entropy in a quantum many-body system, *Nature* **528**, 77 (2015).
- [57] G. Vidal, J. Latorre, E. Rico, and A. Kitaev, Entanglement in quantum critical phenomena, *Phys. Rev. Lett.* **90**, 227902 (2003).
- [58] P. Calabrese and J. Cardy, Entanglement entropy and quantum field theory, *J. Stat. Mech.* **06**, P06002 (2004).
- [59] P. Calabrese and J. Cardy, Entanglement entropy and conformal field theory, *J. Phys. A* **42**, 504005 (2009).
- [60] A. E. B. Nielsen, G. Sierra, and J. I. Cirac, Violation of the area law and long-range correlations in infinite-dimensional-matrix product states, *Phys. Rev. A* **83**, 053807 (2011).
- [61] V. Bois, S. Capponi, P. Lecheminant, M. Moliner, and K. Totsuka, Phase diagrams of one-dimensional half-filled two-orbital $\text{SU}(N)$ cold fermion systems, *Phys. Rev. B* **91**, 075121 (2015).
- [62] V. Bois, P. Fromholz, and P. Lecheminant, One-dimensional two-orbital $\text{SU}(N)$ ultracold fermionic quantum gases at incommensurate filling: A low-energy approach, *Phys. Rev. B* **93**, 134415 (2016).
- [63] S. Capponi, P. Lecheminant, and K. Totsuka, Phases of one-dimensional $\text{SU}(N)$ cold atomic Fermi gases—From molecular Luttinger liquids to topological phases, *Ann. Phys.* **367**, 50 (2016).